Surface diffusion and desorption of exohedral Li^+ from the surface of a fullerene

V. Bernshtein and I. Oref*
Department of Chemistry, Technion–Israel Institute of Technology, Haifa 32000, Israel
(Received 18 August 2000; published 5 March 2001)

Surface diffusion and desorption of Li^+ from the outer surface of C_{60} are explored by quasiclassical trajectory calculations. The dynamics of exohedral Li^+, initially at the center of a ring on the outer cage of C_{60}, is followed as a function of time. Ring hopping between adjacent rings is the major diffusion mechanism but 12–20 % of the ions, depending on the temperature, leave the ring, orbit the molecule, and fall back on a nonadjacent ring. There can be a sequence of hopping and orbiting before total desorption takes place. The average lifetime of an orbit is independent of the temperature, while the exohedral complex lifetime decreases with temperature. Rate coefficients for ring hopping and desorption are reported as a function of temperature. The average kinetic energy removed from the C_{60} by the desorbing ion increases with temperature and it is independent of the lifetime of the complex. Kinetic-energy release distributions at various temperatures are reported.

DOI: 10.1103/PhysRevA.63.043201 PACS number(s): 61.48.+c

INTRODUCTION

Collisions between fullerene molecules and metal or rare-gas ions or between fullerene molecules and rare-gas atoms form stable complexes [1–38]. Two possible complexes can be formed. One type is formed when the ion penetrates the C_{60} cage and resides on the inner wall of the molecule. Such a complex is called an endohedral complex and is denoted by $M^+@C_{60}$ The other type is formed when the ion resides on the outer surface of the molecule. Such a complex is called an exohedral complex and is denoted by M^+C_{60}. These complexes are of current interest and have practical applications. The endohedral complexes find use in nanodevices in as much as they serve as model compounds for nanotube-based devices. The exohedral complexes provide information on surface diffusion and desorption from surfaces.

Collisions of rare-gas ions with C_{60} leading to endohedral complexes have been studied at various collision energies [4–6]. It was found that the dominant mechanism is charge exchange and the inert-gas atom penetrates the C_{60}^+ ion to form an $R@C_{60}^+$ endohedral complex. The insertion efficiency depends on the reactants relative translational energy and can reach values of over 1%. Collisions of alkali-metal ions also lead to endohedral complex formation. In this case there is no charge exchange between the metal ions and the C_{60} because of the low ionization potentials of the metals [7,8]. Insertion occurs also in collisions of accelerated noble-gas ions with surface layers of C_{60} [14]. A similar procedure was used for the insertion of alkali-metal ions into C_{60} [15]. The location of the ion inside the cage depends on the size of the ion. For example, for a Li^+ ion the minimum in the potential-energy surface occurs when the ion is in the center of a pentagonal or hexagonal ring away from the center of mass of the C_{60} molecule [24].

In parallel to the intense experimental activity, numerical calculations have been done in order to explain the experimental results. *Ab initio* calculations [13,18,19] were performed to determine the parameters of the potential-energy surface and the stability of the endohedral system. Ion/C_{60} intermolecular potentials were developed [20–22] and used in molecular-dynamics simulations of experiments. The system [13] He/C_{60}^+ was modeled by using a modified hydrocarbon potential [20] and the trajectories were restricted to a line of approach through the five- and six-member rings in the C_{60}. Good agreement between experiments and simulations was reported [20]. Another molecular-dynamics study [28] on the He^+/C_{60} and Li^+/C_{60} systems did not reproduce the percent insertion found in experiments.

The multiple-well potential-energy surface (PES) of the system determines the location of the ion, which, in turn, determines the spectroscopy of the system [23–26]. Dunlap, Ballester, and Schmidt have calculated the PES for $M^+@C_{60}$ using all-electron local-density-functional total-energy calculations [24(a)]. For the case of the Li^+ ion they find that the minimum in the PES is at 0.14 nm from the center of the cage for the fivefold axis and at 0.12 nm for the threefold axis. The well depth relative to the configuration where the ion is located at the center of the C_{60} is 0.51 eV for both structures. Endohedral vibrations are reported at $\sim$350 cm^{-1}. The results of *ab initio* Hartree-Fock calculations by Varganov, Avramov, and Ovchinnikov [24(b)] also show that the Li^+ is located off center and that the minima in the PES are located in the centers of the pentagonal and hexagonal rings. Joslin *et al.* [25] have used the PES of Dunlap *et al.* [24(a)] to calculate the vibrational-rotational bands of $Li^+@C_{60}$. They find a pure rotation peak near 40 cm^{-1} and a fundamental vibration-rotation band at 350 cm^{-1}. Hernandez-Rojas, Breton, and Llorente [27] used a pairwise Lennard-Jones potential for the endohedral interaction and calculated the rotational spectra of $M^+@C_{60}$. Experiments by Campbell [16(b)] give $\sim$430 cm^{-1} for the endohedral vibration.

In addition to all the static aspects discussed above, there is also a dynamic side to the problem. The endohedral ion is not in one particular PES well but can also be in motion, migrating from one ring to another. Therefore, dynamic

*Electronic mail: chroref@aluf.technion.ac.jl

computational methods are required. Quantum-chemical calculations are the preferable method for studying the dynamics of chemical reactions. However, they are impractical for most systems, especially systems as complex as fullerenes. *Ab initio* molecular-dynamics calculations have been used [24(c,d)] for $Li^+@C_{60}$ but the durations of the dynamic processes were limited to 75 fs, three orders of magnitude shorter than realistic reaction times in endohedral and exohedral systems at temperatures of up to 1500 K. Therefore, quasiclassical trajectory calculations are the choice method to use.

We have used quasiclassical trajectory calculations [29] to study processes that occur in a high-energy collision of Li^+ with C_{60}. The degree of $Li@C_{60}^+$ formation as a function of the relative translational energy was determined and the escape from the cage, following the endohedral formation, was followed as a function of the relative translational energy. The collisional energy-transfer probability density function $P(E',E)$ in inelastic collisions was determined and combined with a RRKM theory rate coefficient $k(E)$ to give the degree of dissociation of the excited C_{60}. In addition, the intramolecular energy redistribution following the initial impact of the Li^+ in the center of a pentagonal ring on the surface of the C_{60} was calculated [17(a)]. We have also performed a detailed quasiclassical trajectory study of the dynamics of Li^+ inside the cage of C_{60} as a function of the temperature of the system [17(b)]. The movement of the ion from one ring to another was depicted as an ''isomerization'' reaction and the rate coefficients k were determined at each temperature. Plots of $\ln k$ vs $1/T$ gave Arrhenius-type behavior up to 900 K. At higher temperatures the ion can fly across the cage without migrating along the inner wall. In such a case the term ''rate coefficient'' loses its meaning altogether and there is an ion moving freely in a potential field.

An open question related to studying chemical reactions by quasiclassical trajectory calculations concerns the flow of zero-point energy (ZPE) from various vibrational modes of the molecule into the reaction coordinate [39–50]. Various methods have been suggested to correct for this deficiency. An analysis and a comparison of some of the methods are given by Lim [48]. In one method all trajectories with internal energy below the ZPE of the products are replaced by new trajectories [43]. In another approach [46], a correction factor proportional to the transition-state sum of states is applied to the calculated rate coefficient of the reaction. Other correction methods are more complicated and involve adjusting the trajectories as the calculations progress [39,41,42,44,45,47–50]. In the ion/C_{60} system there is surface diffusion, or ring hopping, of the Li^+ ion, which is akin to an isomerization reaction and desorption of the weakly bound Li^+. The fact that the presence of Li^+ does not alter the normal-mode frequencies of the C_{60} is an indication that there are very weak Li^+-carbon interactions outside the C_{60} cage. Therefore, there is no question of leakage of ZPE from the C_{60} into the reaction coordinate, neither is there a question of the products of the isomerization having energy below the ZPE, because the energy release in the exit channel is greater than the ZPE of the Li^+-C_{60} modes. The internal energy of the C_{60} with its 174 internal modes is orders of magnitude higher than the kinetic-energy release in the desorption process. This also ensures that the kinetic energy carried by the ion will not deplete the internal modes below the ZPE level.

Exohedral complexes of a metal ion and a C_{60} molecule, the subject of the present work, have also been extensively investigated in solutions [30–32] and in the gas phase [33–38] and studied theoretically [51,52,24(b)]. The theoretical calculations show that the ion is located above the center of a five- or six-membered ring or above a C═C bond [51,52,24(b)]. The most stable configuration is when the ion is located above the center of a hexagonal ring. Hira and Ray [51(a)] used unrestricted Hartree-Fock theory to calculate the energies of the Na^+/C_{60} system. They report that the exohedral well depths are smaller than the endohedral by 0.4 eV with the c_3 symmetry site being the deepest well. For the Li^+/C_{60} system, Ruiz *et al.* [51(c)] used a semiempirical model of the Pariser-Parr-Pople type and multipole expansion of the charge potential at the surface of the C_{60} to obtain potential-energy values. They find that the well depths of the endohedral complex are deeper than the exohedral ones. Varganov, Avramov, and Ovchinnikov [24(b)] use *ab initio* Hartree-Fock calculations and find that the exohedral and endohedral potential wells are of identical depths. Andreoni and Curioni [52] have used density-functional theory to calculate the structure and dynamics of metallofullerenes. They find that the binding energies of Li^+C_{60} are higher than those of $Li^+@C_{60}$ by as much as 7 kcal/mol. De Proft, Van Alsenov, and Geerling [51(b)] calculated a well depth of 9.4 kcal/mol for $Li^+@C_{60}$. These results differ by as much as 60% from other reported values. Basir and Anderson [38] have found experimentally that two kinds of hexahedral complex are formed in collisions of transition-metal ions with C_{60}. At low collision energies the ion resides above the C_{60} and the complex dissociates with loss of the metal ion. At high collision energies the metal ion inserts into the C_{60} structure and the complex decomposes with a loss of MC_2. Our work is related only to Li^+C_{60}, which is formed at low energies.

The dynamics of an ion on the outer surface of C_{60}, an exohedral case, is different from its diffusion along the inner wall of the fullerene molecule [17(b)]. The PES is different and in addition to surface diffusion there is also desorption where the ion leaves the surface of the fullerene molecule altogether. In the present work we explore the rate of Li^+ ion desorption from the surface of C_{60} and the rate of diffusion of Li^+ on the surface of C_{60}, and report the rate coefficients for both processes as a function of temperature.

THEORY

The numerical methods used in the present work are reported in [53] and [54]. The equations of motion were integrated by using a modified public domain program VENUS [55]. As reported in the Introduction, the intermolecular potential varies in magnitude and trend. We have used a carbon/ion pairwise potential [21,28] that was used in our previous work on $Li^+@C_{60}$ [17]. It combines the repulsive part of a Lennard-Jones potential with an ion-atom attractive

part whose $1/r^4$ dependence is derived from the Hellmann-Feynman theorem [28]:

$$V_{\text{C-ion}} = 4\epsilon[(\sigma_{\text{Ci}}/r)^{12}/z^2 - (\sigma_{\text{Ci}}/r)^4], \tag{1}$$

where $\epsilon = 78.4\,\text{meV}$ [22], $\sigma_{\text{Ci}} = (\sigma_{\text{C}} + \sigma_{\text{Li}^+})/2$, $\sigma_{\text{C}} = 0.284\,\text{nm}$, $\sigma_{\text{Li}^+} = 0.136\,\text{nm}$, and z is the ionic charge.

The intramolecular harmonic potential includes all the normal-mode contributions, stretching, bending, and nonbonded interactions between second-neighbor atoms [22]. A reasonable approximation is to apply one force constant for all the short C-C distances and one for the long C-C distances. The same approximation was used for the bending force constants. The values of the parameters of this potential were obtained from Procacci *et al.* [22]. The Li^+-C_{60} transition modes were calculated together with the molecular modes by including the intermolecular potential as part of the intramolecular potential. The initial rotational energy was chosen from the appropriate thermal energy distributions. The internal energy was the average quantum-statistical thermal energy of the exohedral complex at each temperature. Two energetically stable initial configurations were chosen: with the ion above the center of a five- or a six-membered ring.

Ion migration on the surface was considered as an isomerization reaction where the ion above the center of a five-membered ring migrated to any of the five neighboring six-membered rings $(5 \rightarrow 6)$ or when the ion above the center of a six-membered ring migrated to one of the three neighboring five-membered rings $(6 \rightarrow 5)$ or to one of the three neighboring six-membered rings $(6 \rightarrow 6)$. In addition to isomerization there is also desorption. Local desorption occurs when the ion leaves the surface. There are two outcomes to local desorption: it can desorb from one ring and land on another, or it can leave the molecule altogether. Each of these processes is considered separately.

A schematic representation of the diffusion/desorption processes is depicted in the following diagram.

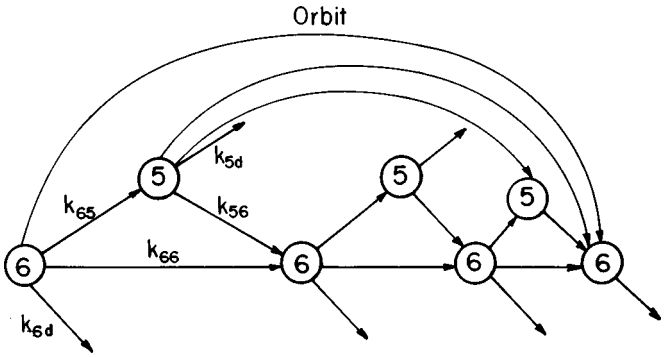

In this diagram, the numbers 5 and 6 describe a five- and a six-membered ring, respectively. The first number in the subscript of the rate coefficient indicates the starting ring and the second number indicates the destination ring. Thus, k_{65} is the rate coefficient of jumping from a six- to a five-membered ring and k_{id} is the rate coefficient for desorption where i indicates a five- or a six-membered ring.

The reaction coordinate for each process was determined from the PES and it was verified that it is the minimum-potential-energy path. The product of a reaction was defined by its final configuration. The distances between the ion and the carbon atoms surrounding it were calculated during the trajectory and, when the distances between the ion and the carbon atoms in the product configuration were shorter than those of the reactant, the reaction was terminated. Local desorption was defined by a distance of 0.335 nm between the ion and its nearest carbon atom. At this distance the intermolecular potential approaches zero. Total desorption is defined as a case when the ion does not return to the surface of the ring after undergoing local desorption.

The $5 \rightarrow 6$ isomerization and desorption is a unimolecular reaction where the rate coefficient $k_5 (= k_{56} + k_{5d})$ is given by

$$\frac{d \ln(N_{\text{nr}}/N_{\text{tot}})}{dt} = -k_5, \tag{2}$$

where N_{nr} is the number of nonreactive trajectories at time t and N_{tot} is the total number of trajectories, which in our calculations was about 5000. For the $6 \rightarrow 5$, $6 \rightarrow 6$, and $6 \rightarrow d$ cases, with rate coefficients k_{65}, k_{66}, and k_{6d}, respectively, the overall rate coefficient k_6 $(= k_{65} + k_{66} + k_{6d})$ is also given by an equation similar to Eq. (2). The individual rate coefficients k_{56} and k_{5d}, k_{65}, k_{66}, and k_{6d} are given by

$$N_r(ij) = \frac{k_{ij} N_{\text{tot}}}{k_i}[1 - \exp(-k_i t)], \tag{3}$$

where i indicates the starting ring and j indicates the destination five- or six-membered ring or desorption. $N_r(ij)$ indicates the number of reactive trajectories starting from ring i and leading to ring j or to desorption and k_i is k_5 or k_6. The trajectory data were plotted as required by Eqs. (2) and (3) and the data were fitted by a linear least-squares fitting. The values of the rate coefficients are the slopes of the lines.

Trajectory calculations yield directly individual rate coefficients that describe ion hopping from one ring to another or desorption from a ring. However, the experimental quantity is the total desorption of the ion from the fullerene, k_d, and it is an integration of individual events where the ion departs from a five- or a six-membered ring regardless of the previous history of how many jumps the ion performed before arriving at the present ring. That is to say, there can be a succession of jumps from one ring to another that ends in ion desorption. In addition, a binary cluster is possible where the ion hovers over the molecule for a given time and falls back on top of one of the rings. The overall lifetime of the ion on the surface is related to the number of jumps on the surface of the molecule and to the duration of the orbiting binary cluster. Below, we discuss the results of our calculations on desorption and surface migration of a Li^+ ion on the outer surface of a C_{60} molecule.

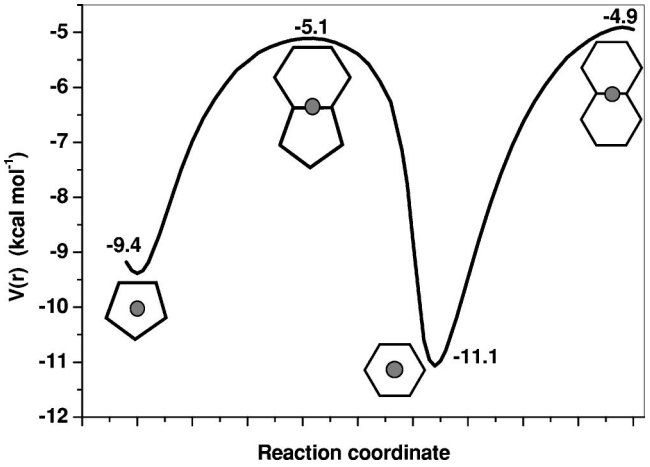

FIG. 1. The reaction coordinate describing the minimum-energy path for surface diffusion of Li^+ on the outer surface of C_{60}. The full circle is the ion.

RESULTS AND DISCUSSION

The reaction coordinate is calculated from the ion-atom intermolecular potential, which is given by Eq. (1), and is shown in Fig. 1. The deepest well is -11.0 kcal/mol and it occurs when the ion is located above the center of a six-membered ring. There is a shallower well of -9.4 kcal/mol when the ion is located above a five-membered ring. A systematic evaluation of the PES shows that the minimum in the potential occurs when the ion moves along the center-center line. This is the reaction coordinate that is shown in Fig. 1. The barrier for $5\rightarrow6$ diffusion is 4.3 kcal/mol, for $6\rightarrow5$ diffusion it is 4.9 kcal/mol, and for $6\rightarrow6$ diffusion it is 5.1 kcal/mol. For desorption, the barriers are the well depths as shown in the drawing of the reaction coordinate.

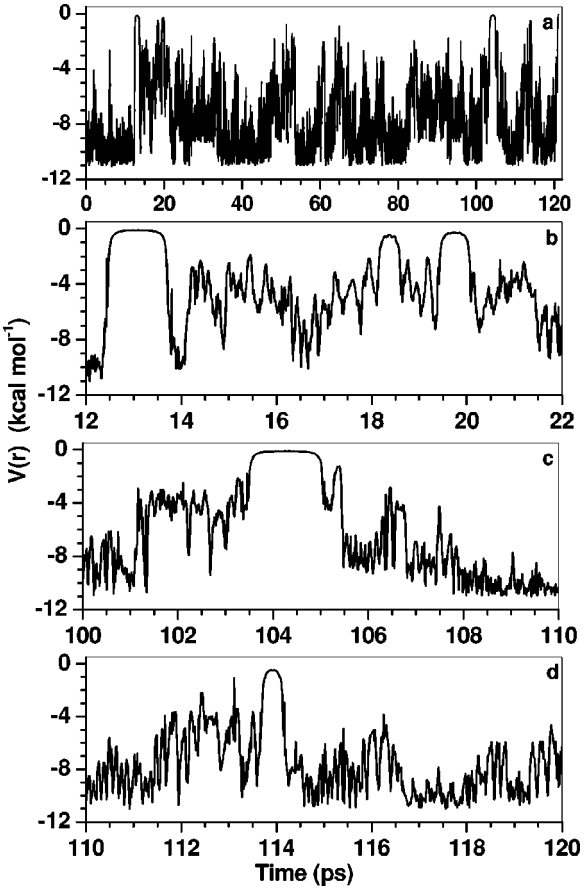

FIG. 2. (a) A trajectory describing the temporal evolution of the potential energy. (b)–(d) describe time segments of the trajectory in (a). The temperature is 1050 K.

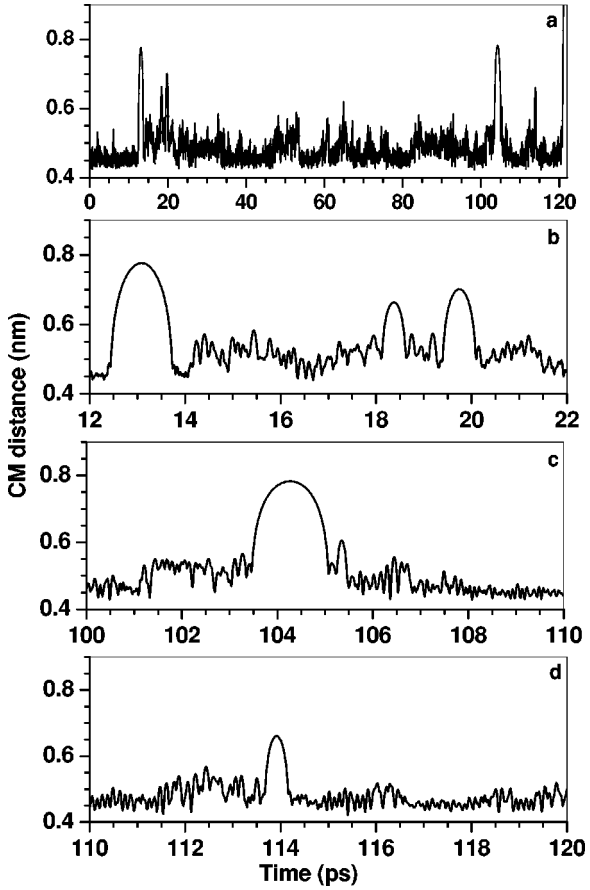

FIG. 3. (a) A trajectory describing the temporal evolution of the distance between the ion and the center of mass (CM) of C_{60}. (b)–(d) describe time segments of the trajectory in (a). The temperature is 1050 K.

The processes of isomerization, orbiting, and desorption are demonstrated by a sample trajectory in Figs. 2 and 3. In the former, the potential energy is shown as a function of time. The temporal evolution of the ion migration during the trajectory is shown in Fig. 2(a). There are random jumps from one well to another. A baseline at -11 kcal/mol indicates that the ion is above a hexagonal ring and a baseline at -9.4 kcal/mol indicates that the ion is above a pentagonal ring. In addition, there are jumps out of the wells leading to the ion orbiting the fullerene molecule with almost zero potential energy. Figures 2(b)–2(d) show expanded time intervals of segments of the trajectory in Fig. 2(a) where the various processes can be better observed. As can be seen, isomerization occurs in a random fashion and the energy needed for the process does not exceed the barrier height by much. In some cases large peaks can be seen. This happens

TABLE I. Percent trajectories that show orbiting of Li^+ above a C_{60} molecule. Initially, the Li^+ is above a hexagonal ring. N^1_{orb} is the number of ions with only one orbit prior to desorption.

T (K)	950	1000	1050	1100	1150	1200	1300	1500
$N^{total}_{orb}/N^{total}_{traj}$ (%)	20.0	19.4	18.7	15.0	15.9	12.0	14.7	12.5
$\langle \tau_{orb} \rangle$ (ps)	0.589	0.598	0.687	0.625	0.644	0.608	0.578	0.616
$N^1_{orb}/N^{total}_{orb}$ (%)	79.6	82.4	84.5	86.2	87.6	89.8	91.6	93.2

when the transition modes attain large quantities of energy, albeit not enough for the ion to be kicked out. There are cases, however, where enough energy is available for the ion to escape the well and orbit the molecule. Peaks that reach the zero-potential-energy level denote these events. An energetic kick will remove the ion altogether from the surface of the molecule.

Figure 3 shows the temporal evolution of the distance between the ion and the center of mass of the fullerene molecule. The shortest distance is when the ion is located above a hexagonal ring. The distance is somewhat larger when the ion is above a five-membered ring. The ion spends a given amount of time in a well above a ring and then hops to another and so on. Orbiting occurs when the ion is kicked hard enough and flies to a distance of 0.8 nm where the potential energy is essentially zero. The trajectory is symmetric and the ion returns to the surface after spending between ~0.5 and ~2 ps in ''space'' above the ring. The average lifetime of an orbit is ~0.6 ps and it is essentially independent of temperature because orbiting occurs when the potential is almost zero regardless of the initial conditions in the complex. Although desorption and surface diffusion from ring to ring are intuitively expected, the high frequency of the orbiting phenomenon is somewhat of a surprise. Table I gives the percent of trajectories with orbiting. At 950 K, 20% of all trajectories show at least one orbiting event. This drops to 12% at 1500 K. The drop in the number of orbiting events with increasing temperature can be explained by the fact that at low temperatures the internal energy is low and there is not enough energy in the transition modes to kick the ion out. As the temperature increases the percent orbiting decreases while total desorption increases.

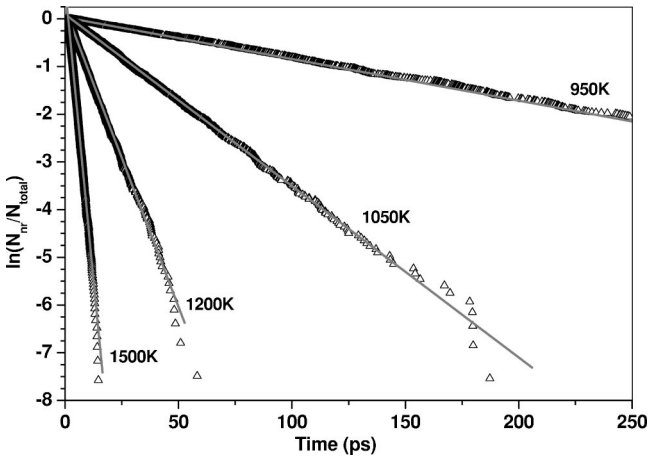

FIG. 4. First-order plots of total desorption of Li^+ from the surface of C_{60}.

The process of hopping and partial orbiting ends when the ion is kicked out with enough energy to overcome the binding energy and desorption occurs. A plot of the logarithm of the number of undesorbed ions versus time, as in Eq. (1), should give the rate coefficient for desorption. Figure 4 shows first-order desorption plots at various temperatures. Also given are the best fits to the data from which the rate coefficients for desorption were obtained. The Arrhenius plot of the rate coefficient for desorption is given in Fig. 5. The temperature dependence of the rate coefficient for desorption is given by $k \approx (5.8 \pm 3.0) \times 10^{14} \exp[(-10.3 \pm 0.8)/T]$. The results are summarized in Table II. The activation energy for desorption is larger than the reaction coordinate barrier height for dissociation of 11.0 kcal/mol that is obtained from potential-energy calculation and reported in Fig. 1.

As mentioned before, an ion located above a ring, in the bottom of the well, can diffuse to another ring or it can desorb by escaping from the surface. Such an event has two outcomes. In one, the ion leaves the fullerene permanently and in the other, when it does not attain enough energy, it falls back after hovering for a while above the molecule. The rate coefficient for desorption from a ring includes both events while the total rate coefficient for desorption, which is the more relevant experimental quantity, represents final desorption from the molecule regardless of the history of the ion prior to the desorption event. The individual rate coefficients for desorption and diffusion, k_{5d}, k_{6d}, k_5, and k_6, as well as k_{65} and k_{66}, were extracted by plotting the appropriate quantities in Eq. (3). Sample plots are given in Fig. 6 and the relevant data are given in Table III. As might be expected, the ratio of surface migration to desorption decreases

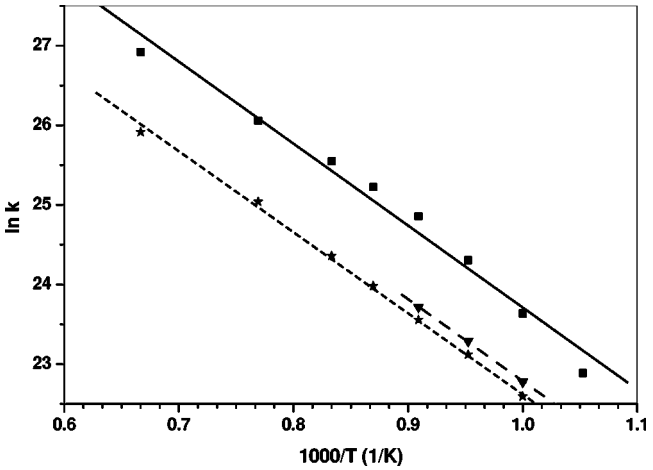

FIG. 5. An Arrhenius plot for trajectory calculations of total desorption of Li^+ from the surface of C_{60} (■); RRKM theory (▼); absolute rate theory (★).

TABLE II. Total desorption of Li^+ from a C_{60} molecule. The Li^+ is initially above a hexagonal ring. Trajectory time limit is 250 ps. E_v is the internal energy at T. N_{tot} is the total number of trajectories; N_d the percent leading to desorption.

T (K)	E_v (kcal mol^{-1})	N_{tot}	N_d (%)	k_d (ps^{-1})
950	161.1	1000	87	8.73×10^{-3}
1000	175.7	1200	99	1.84×10^{-2}
1050	190.5	2000	100	3.60×10^{-2}
1100	205.6	1500	100	6.56×10^{-2}
1150	220.8	1000	100	9.01×10^{-2}
1200	236.1	2000	100	1.25×10^{-1}
1300	267.2	1500	100	2.07×10^{-1}
1500	330.7	4000	100	4.91×10^{-1}

as the temperature increases. The internal energy of C_{60} increases with temperature and with it increases the probability of attaining enough energy in the transition modes to kick the ion out. This can be seen in Fig. 7 where a sharp decrease in the average lifetime of the exohedral complex is observed as a function of temperature.

At 700 K there is no local desorption from the C_{60} during the 300 ps maximum lifetime of the trajectories. At 900 K there is 0.5% of local desorption and no, or very little, total desorption from the C_{60} while at 1500 K 25% of the trajectories undergo local desorption. The dependence of the rate coefficients on temperature is shown in the Arrhenius plots in Fig. 8. The temperature dependences of the rate coefficients are $k_6=(11.0\pm4.8)\times10^{14}\exp[(-9.2\pm0.8)/T]$; $k_{65}=(7.9\pm4.0)\times10^{14}\exp[(-9.5\pm0.9)/T]$; $k_{66}=(9.6\pm5.7)\times10^{14}\exp[(-9.8\pm0.8)/T]$; and $k_{6d}=(10.6\pm5.3)\times10^{15}\exp[(-14.0\pm0.8)/T]$. It should be pointed out that if one waits long enough there will also be total desorption at 700 K. However, it requires long trajectories, which are time and resource expensive. Indication of the degree of total desorption at 700 K could be obtained from an extrapolation of the Arrhenius plot shown in Fig. 5.

As the ion leaves the molecule, it carries with it kinetic energy. This energy is in excess of the C_{3v} potential well depth of 11 kcal/mol (3860 cm^{-1}), all of which is lost by the C_{60} molecule. Kinetic-energy (KE) release distribution

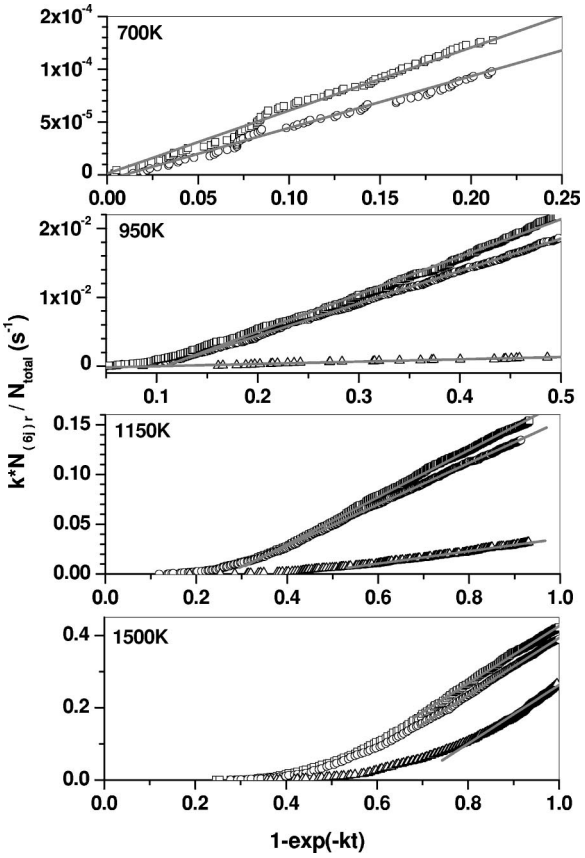

FIG. 6. Plots of Eq. (3) for surface migration of the ion from a hexagonal ring to a pentagonal or a hexagonal ring. The slopes of the lines yield the individual rate coefficients.

curves for sample temperatures are shown in Fig. 9. As might be expected, the KE release curve at 950 K is narrower than the curve at 1500 K. There are a few trajectories with negative KE, which result from the fact that some trajectories are created, at $t=0$, with KE in the well and thus subtracting the well depth sometimes gives negative values that have no physical meaning. These results are in quantitative agreement with those of our previous work on the dissociation of benzene-Ar clusters [56]. The average KE release increases with the temperature as shown in Fig. 10, which shows the average energy that is removed from the C_{60} molecule as a

TABLE III. Isomerization/desorption from a single hexagonal ring as a function of temperature. E_v is the internal energy at T. N indicates the number of trajectories. For the meaning of the subscripts see the text. Trajectory time limit is 7.5 ps.

T (K)	E_v (kcal mol^{-1})	N_{tot}	N_{65} (%)	N_{66} (%)	N_{6d} (%)	k_6 (ps^{-1})	k_{65} (ps^{-1})	k_{66} (ps^{-1})	k_{6d} (ps^{-1})
700[a]	92.3	1000	15.0	12.0		1.08×10^{-3}	5.97×10^{-4}	4.90×10^{-4}	
900	146.7	4840	14.5	12.0	0.5	5.10×10^{-2}	3.00×10^{-2}	2.43×10^{-2}	
950	161.1	2322	23.7	20.2	1.4	9.18×10^{-2}	5.44×10^{-2}	4.70×10^{-2}	3.35×10^{-3}
1050	190.5	2312	35.4	33.2	4.5	2.03×10^{-1}	1.20×10^{-1}	1.16×10^{-1}	1.90×10^{-2}
1150	220.8	2884	42.8	38.7	8.9	3.60×10^{-1}	2.36×10^{-1}	2.08×10^{-1}	6.27×10^{-2}
1500	330.7	4342	39.0	35.9	24.8	1.08	7.92×10^{-1}	7.94×10^{-1}	8.10×10^{-1}

[a]Trajectory time limit is 300 ps.

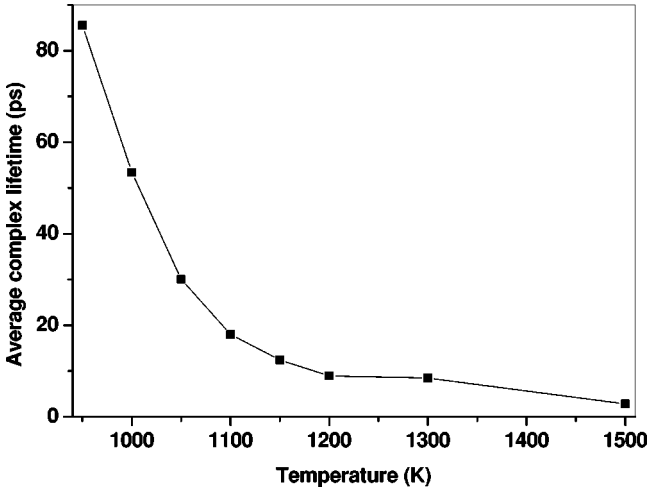

FIG. 7. Average complex lifetime as a function of temperature. The solid line is a visible aid.

function of the temperature. The temperature dependence of the average energy removed from the C_{60} molecule is given by $-\langle \Delta E \rangle = 3761 \pm 43 + (0.624 \pm 0.037)T$. Subtracting the well depth yields the average KE released in desorption of a Li^+ ion from the surface of the molecule. There is no correlation between the lifetime of the exohedral complex and the amount of energy removed by the ion. This can be seen in Fig. 11, where the average energy removed from the molecule is given as function of the complex lifetime. The lack of correlation between the two quantities can be explained by the fact that the mechanism of desorption involves an energetic kick by an out-of-plane mode or modes without regard to past history. Figure 11 implies statistical dissociation of the exohedral complex and calls for using statistical theories for calculating the rate coefficient for desorption.

In order to compare trajectory results with statistical theories we have calculated the rate coefficient for total desorption by activated complex theory (ACT) and by RRKM

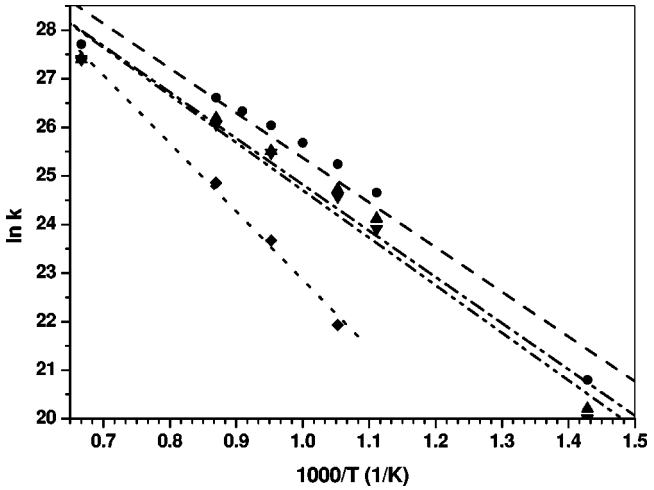

FIG. 8. Arrhenius plots for local desorption and surface diffusion of Li^+ from a hexagonal ring on the surface of C_{60}; $6 \rightarrow d$ (♦), $6 \rightarrow 5$ (▲), $6 \rightarrow 6$ (▼), and overall rate of all three processes (●).

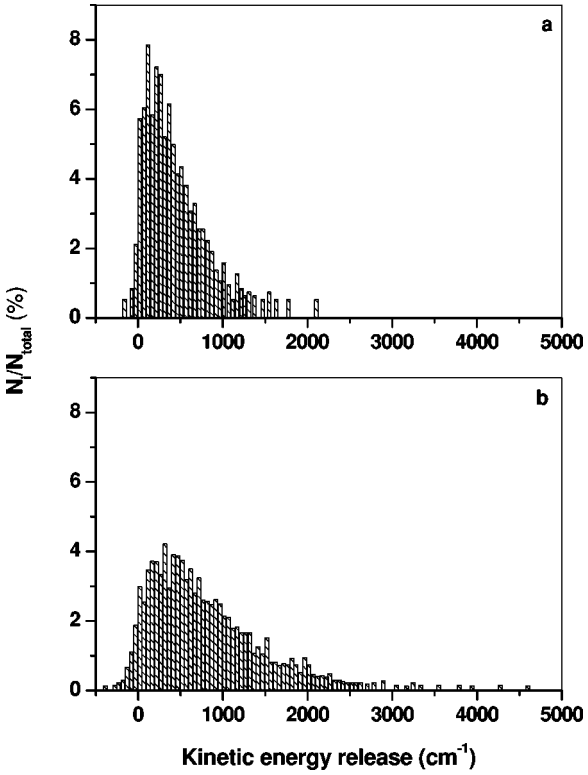

FIG. 9. Kinetic-energy release histograms at (a) 950 and (b) 1500 K.

theory using as the activation energy the slope of the line that was obtained from the trajectory results in Fig. 5. The results are also presented in Fig. 5. As can be seen, there is good agreement between the trajectory results and the ACT and RRKM results. There is a discrepancy, however, between the depth of the well in the PES and the slope of the lines in Fig. 5.

It is interesting to compare the dynamics of the movement of a Li^+ ion on the outer surface of C_{60}, the exohedral case, to the dynamics of diffusion along the inner walls of the fullerene molecule, the endohedral case [17(b)]. The local

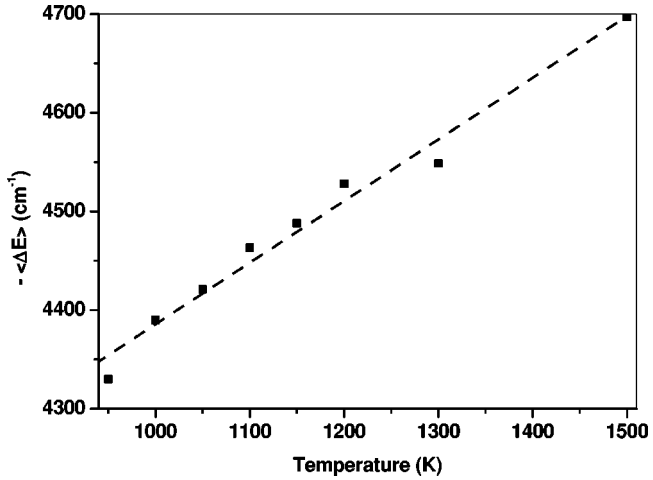

FIG. 10. The average energy removed by the dissociating Li^+ as a function of temperature. Dashed line is best fit to the data.

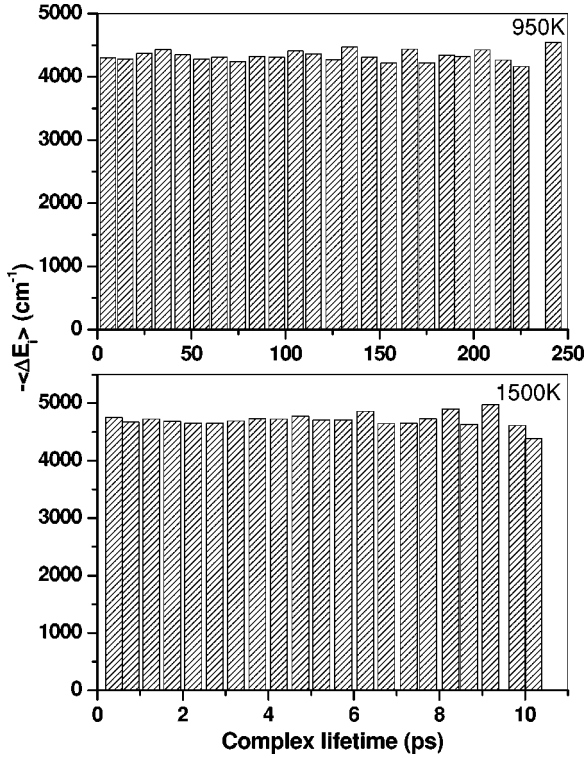

FIG. 11. The average energy removed by the dissociating Li^+ as a function of the exohedral complex lifetime.

environment is different for the two cases and therefore the PES is different. The energy barriers for $6\rightarrow5$ and $6\rightarrow6$ isomerizations of exohedral ions are higher by a factor of 3 than those for isomerizations of endohedral ions. In both cases, surface diffusion occurs by the ion jumping from one ring to another but, since the barriers for surface diffusion are different, the rate coefficients for diffusion are different. In addition, a fair fraction of the exohedral ions undergo diffusion by orbiting, that is to say, jumping and skipping over a few rings and landing on a ring that is not a nearest neighbor to the ring of origin. While orbiting does not take place in endohedral complexes, at high temperature the ion rattles inside the cage, not diffusing but flying from one side to another. There is also the obvious case that in addition to surface diffusion in exohedral complexes there is also desorption, where the ion leaves the surface of the fullerene molecule altogether. This does not happen in the endohedral case. In short, in spite of the fact that an identical pairwise potential is used in both types of complex, a different dynamic behavior is observed inside and outside the cage of C_{60}.

In conclusion, we have investigated surface diffusion and desorption of exohedral Li^+ from C_{60}. Diffusion occurs by ring hopping (the ion jumps from one ring to its nearest-neighbor ring), or by orbiting (where the ion skip-jumps and lands on a non-nearest-neighbor ring). Orbiting is an important mechanism for diffusion and comprises 20% of all diffusion events at 950 K and 12% at 1500 K. The decline in the number of orbiting events at high temperatures is due to the fact that more ions desorb and fewer ions are available for orbiting. The average time an ion spends in orbit is 0.6 ps and it is independent of the temperature because orbiting represents an energy window with zero potential energy. At high temperatures, more energetic kicks are expected but they cause desorption and not orbiting, which represents only a segment of all events with common history at all temperatures. Rate coefficients for surface diffusion and desorption as a function of temperature are provided. The trajectory results for desorption are compared with rate coefficients calculated by RRKM and activated complex theories. Average exohedral complex lifetimes are given and are shown to decline with temperature. The kinetic energy acquired by the departing ion is given by kinetic-energy release histograms. As expected, the average kinetic energy of the ion increases with temperature. There is no correlation between the exohedral complex lifetime and the amount of energy removed by the ion. This indicates that the desorption mechanism is instantaneous and depends on a fast final kick. This was verified by animation of numerous trajectories. The details provided above give a comprehensive understanding of the mechanism of diffusion and desorption of Li^+ from the surface of C_{60}.

ACKNOWLEDGMENTS

This work was supported by the Technion V.P.R. Fund, by the B. and N. Ginsburg Energy Research Fund, by the fund for promotion of research at the Technion, and by the Ministry of Science and the Arts.

[1] E. B. Cambell and F. Rohmund, Rep. Prog. Phys. **63**, 1061 (2000).
[2] (a) M. Saunders, H. A. Jimenez-Vasques, R. J. Cross, and R. J. Poreda, Science **259**, 1428 (1993); (b) M. Saunders, H. A. Jimenez-Vasques, R. J. Cross, S. Mroczkowski, M. Cross, D. E. Giblin, and R. J. Poreda, J. Am. Chem. Soc. **116**, 2193 (1994).
[3] M. Saunders, R. J. Cross, H. A. Jimenez-Vasques, R. Shimshi, and A. Khong, Science **271**, 1693 (1996).
[4] Z. Wan, J. F. Christian, and S. L. Anderson, J. Chem. Phys. **96**, 3344 (1992).
[5] J. F. Christian, Z. Wan, and S. L. Anderson, J. Chem. Phys. **99**, 3468 (1993).
[6] Y. Basir and S. L. Anderson, J. Chem. Phys. **107**, 8370 (1997).
[7] Z. Wan, J. F. Christian, and S. L. Anderson, Phys. Rev. Lett. **69**, 1352 (1992).
[8] Z. Wan, J. F. Christian, Y. Basir, and S. L. Anderson, J. Chem. Phys. **99**, 5858 (1993).
[9] T. Weiske, D. K. Bohme, J. Hrusak, W. Kratschmer, and H. Schwarz, Angew. Chem. **103**, 989 (1991).
[10] T. Weiske, D. K. Bohme, J. Hrusak, W. Kratschmer, and H. Schwarz, Angew. Chem. Int. Ed. Engl. **30**, 884 (1991).
[11] M. M. Ross and J. H. Callahan, J. Phys. Chem. **95**, 5720 (1991).

[12] T. Wong, J. K. Terlouw, T. Weiske, and H. Schwarz, Int. J. Mass Spectrom. Ion Processes **113**, 23 (1992).
[13] R. C. Mowrey, M. Ross, and J. H. Callahan, J. Phys. Chem. **96**, 4755 (1992).
[14] R. Shimshi, R. J. Cross, and M. Saunders, J. Am. Chem. Soc. **119**, 1163 (1997).
[15] R. Tellgmann, N. Krawez, S. H. Lin, I. V. Hertel, and E. E. B. Campbell, Nature (London) **382**, 407 (1996).
[16] (a) E. E. B. Campbell, R. Tellgmann, N. Krawez, and I. V. Hertel, J. Phys. Chem. Solids **58**, 1763 (1997); (b) E. E. B. Campbell (private communication).
[17] V. Bernshtein and I. Oref, (a) Chem. Phys. Lett. **313**, 52 (1999); (b) Phys. Rev. A **62**, 033201 (2000).
[18] L. Pang and F. Brisse, J. Phys. Chem. **97**, 8562 (1993).
[19] S. Patchkovskii and W. Thiel, J. Chem. Phys. **106**, 1796 (1997).
[20] D. W. Brenner, Phys. Rev. B **42**, 9458 (1990).
[21] J. Breton, J. Gonzales-Platas, and C. Girardet, J. Chem. Phys. **99**, 4036 (1993).
[22] P. Procacci, G. Cardini, P. Salvi, and V. Schettino, Chem. Phys. Lett. **195**, 347 (1992).
[23] J. L. Ballester and B. I. Dunlap, Phys. Rev. A **45**, 7985 (1992).
[24] (a) B. I. Dunlap, J. L. Ballester, and P. P. Schmidt, J. Phys. Chem. **96**, 9781 (1992); (b) S. A. Varganov, P. V. Avramov, and S. G. Ovchinnikov, Fiz. Tverd. Tela St. Petersburgh **42**, 378 (2000) [Phys. Solid State **42**, 388 (2000)]; (c) K. Ohno, Y. Maruyama, K. Esfarjani, Y. Kawazoe, N. Sato, R. Hatakeyama, T. Hirata, and M. Niwano, Phys. Rev. Lett. **76**, 3590 (1996); (d) A. A. Farajian, K. Onho, K. Esfarjani, Y. Maruyama, and Y. Kawazoe, J. Chem. Phys. **111**, 2164 (1999).
[25] C. G. Joslin, J. Yang, C. G. Grey, S. Goldman, and J. D. Poll, Chem. Phys. Lett. **208**, 86 (1993).
[26] C. G. Joslin, C. G. Grey, S. Goldman, J. Yang, and J. D. Poll, Chem. Phys. Lett. **215**, 144 (1993).
[27] J. Hernandez-Rojas, J. Breton, and J. M. Gomez Llorente, J. Chem. Phys. **104**, 1179 (1996).
[28] T. Kaplan, M. Rasolt, M. Karimi, and M. Mostoller, J. Phys. Chem. **97**, 6124 (1993).
[29] V. Bernstein and I. Oref, J. Chem. Phys. **109**, 9811 (1998).
[30] P. Fagan, J. Calabrese, and B. Malone, Acc. Chem. Res. **25**, 134 (1992).
[31] A. Hirsch, Synthesis **8**, 895 (1995).
[32] W. Sliwa, Transition Met. Chem. **21**, 583 (1996).
[33] L. M. Roth, Y. Huang, J. T. Shwedler, C. J. Cassaday, D. Ben-Amotz, B. Kahr, and B. S. Freiser, J. Am. Chem. Soc. **113**, 6298 (1991).
[34] S. W. McElvany, J. Phys. Chem. **96**, 4935 (1992).
[35] V. Baranove and D. Boheme, Int. J. Mass Spectrom. Ion Processes **149/150**, 543 (1995).
[36] Y. J. Bashir, Z. Wan, J. F. Christian, and S. L. Anderson, Int. J. Mass Spectrom. Ion Processes **138**, 173 (1994).
[37] Y. Basir and S. L. Anderson, Chem. Phys. Lett. **243**, 45 (1995).
[38] Y. Basir and S. L. Anderson, Int. J. Mass. Spectrom. **185-7**, 603 (1999).
[39] J. M. Bowman, B. Gazdy, and Q. Sun, J. Chem. Phys. **91**, 2859 (1989).
[40] W. H. Miller, W. L. Hase, and C. L. Darling, J. Chem. Phys. **91**, 2863 (1989).
[41] G. H. Peslherbe and W. L. Hase, J. Chem. Phys. **100**, 1179 (1994).
[42] M. Ben-Nun and R. D. Levine, J. Chem. Phys. **101**, 8768 (1994).
[43] A. J. Varandas and J. M. C. Marques, J. Chem. Phys. **100**, 1908 (1994).
[44] K. F. Lim and D. A. McCormack, J. Chem. Phys. **102**, 1705 (1995).
[45] D. A. McCormack and K. F. Lim, J. Chem. Phys. **103**, 1991 (1995).
[46] D. L. Shen and H. O. Pritchard, J. Chem. Soc., Faraday Trans. **92**, 4357 (1996).
[47] D. A. McCormack and K. F. Lim, J. Chem. Phys. **107**, 572 (1997).
[48] K. F. Lim, J. Chem. Soc., Faraday Commun. **93**, 669 (1997).
[49] D. A. McCormack and K. F. Lim, Phys. Chem. Chem. Phys. **1**, 1 (1999).
[50] (a) G. Stock and U. Moeller, J. Chem. Phys. **111**, 65 (1999); (b) **111**, 77 (1999).
[51] (a) S. H. Hira and A. K. Ray, Phys. Rev. A **52**, 141 (1995); (b) F. De Proft, C. Van Alsenov, and P. Geerlings, J. Phys. Chem. **100**, 7440 (1996); (c) A. Ruiz, J. Hernandez-Rojas, J. Breton, and J. M. Gomez Llorente, J. Chem. Phys. **109**, 3573 (1998).
[52] W. Andreoni and A. Curioni, Appl. Phys. A: Mater. Sci. Process. **66**, 299 (1998).
[53] V. Bernshtein, K. F. Lim, and I. Oref, J. Phys. Chem. **99**, 4531 (1995).
[54] D. C. Clary, R. G. Gilbert, V. Bernshtein, and I. Oref, Faraday Discuss. **102**, 423 (1995).
[55] W. L. Hase, R. J. Duchovic, X. Hu, A. Komornicki, K. F. Lim, D.-H. Lu, G. H. Peslherbe, K. N. Swamy, S. R. Vande-Linde, A. Varandas, H. Wang, and R. J. Rolf, Quantum Chem. Program Exch. Bull. **16**, 43 [QCPE Program 671] (1996).
[56] V. Bernshtein and I. Oref, J. Chem. Phys. **112**, 686 (2000).